AIAA JOURNAL
Vol. 33, No. 6, June 1995

Integration of Navier–Stokes Equations Using Dual Time Stepping and a Multigrid Method

Andrea Arnone*
University of Florence, Florence, Italy
and
Meng-Sing Liou† and Louis A. Povinelli‡
NASA Lewis Research Center, Cleveland, Ohio 44135

Efficient acceleration techniques typical of explicit steady-state solvers are extended to time-accurate calculations. Stability restrictions are greatly reduced by means of a fully implicit time discretization. A four-stage Runge–Kutta scheme with local time stepping, residual smoothing, and multigridding is used instead of traditional computationally expensive factorizations. Two applications to natural unsteady viscous flows are presented to check for the capability of the procedure.

Introduction

RECENT progress in computational fluid dynamics along with the evolution of computer performance encourages scientists to look in to details of flow physics. There are practical applications where the unsteadiness of the problem can not be neglected (i.e., vortex shedding, natural unsteadiness, forced unsteadiness, aeroelasticity, turbomachinery rotor–stator interaction). Up to now, most of the analysis and designing tools are based on a steady or quasi-steady assumption, even if the flow is known to be unsteady. Today, due to the improvement in computer resources, there is a strong interest in developing methodologies for efficient and reliable simulation of unsteady flow features.

It is a common experience, while using time-accurate explicit schemes, to be forced to choose the time step on the basis of stability restrictions. As a consequence, unless the problem is a very high frequency one, the number of time steps to be performed is much higher than the one required for time accuracy.

By means of some implicit factorization, stability restrictions can be relaxed, but the work required at each time step grows rapidly with grid dimension and complexity of the flow equations. In addition, application of boundary conditions in a fully implicit manner is difficult.

In viscous flow calculations, the grid is clustered close to the shear layer and the characteristic time step varies several orders of magnitude inside the computational domain. Even if in several practical applications the characteristic time step of the core-flow region is comparable with the one required by time accuracy, close to the walls the time step restrictions become extremely severe. Therefore, highly vectorizable schemes with less stability restrictions on the allowable time step would be an interesting combination.

Explicit schemes combined with acceleration techniques have proven to be very effective for solving steady problems.[1–3] Unfortunately, the computational efficiency of those time-marching solvers is achieved by sacrificing the accuracy in time. In this paper, it is shown that the conventional steady-state acceleration techniques, specifically the multigrid techniques, can still be applied to unsteady viscous problems. The basic idea is to introduce a dual time stepping and to reformulate the governing equations so that they can be handled by an explicit accelerated scheme.[4] If the time discretization is made implicit, stability restrictions are removed and acceleration techniques can be used instead of traditional time-consuming factorizations (i.e., alternate directional implicit and lower/upper).

Received Nov. 6, 1993; revision accepted Dec. 28, 1994; accepted for publication Dec. 28, 1994.

*Assistant Professor, Department of Energy Engineering.
†Senior Scientist, Internal Fluid Mechanics Division. Associate Fellow AIAA.
‡Deputy Chief, Internal Fluid Mechanics Division. Fellow AIAA.

As the final goal of the present research is the study of unsteady phenomena in turbomachinery components, such as rotor–stator interaction and stage analysis, the technique was implemented in the TRAF(2D/3D) codes.[3,5] These two- and three-dimensional solvers were developed during a joint project between the University of Florence and NASA Lewis and were designed for turbomachinery blade row analysis.

The procedure is validated by applying it to two examples of natural unsteady two-dimensional viscous flows.

Governing Equations

The two-dimensional, unsteady, Reynolds-averaged Navier–Stokes equations are written in conservative form in a curvilinear coordinate system ξ, η as

$$\frac{\partial (J^{-1}Q)}{\partial t} + \frac{\partial \boldsymbol{F}}{\partial \xi} + \frac{\partial \boldsymbol{G}}{\partial \eta} = \frac{\partial F_v}{\partial \xi} + \frac{\partial G_v}{\partial \eta} \tag{1}$$

where the vectors $\boldsymbol{F}$ and $\boldsymbol{G}$ account for the convective terms whereas the viscous terms are included in F_v and G_v. J is the Jacobian of the transformation and t the time. The pressure is obtained from the equation of state, and the eddy-viscosity hypothesis is used to account for the effect of turbulence. The turbulent quantities are computed using the algebraic model of Baldwin and Lomax.[6]

Spatial Discretization and Artificial Dissipation

In finite volume approach, the governing equations are discretized in space starting from an integral formulation and without any intermediate mapping. In the present work, due to the extensive use of eigenvalues and curvilinear quantities, we found it more convenient to map the Cartesian space (x, y) onto a generalized curvilinear one (ξ, η). In the curvilinear system, the equation of motion (1) can be easily rewritten in integral form by means of Green's theorem, and the metric terms are handled following the standard finite volume formulation. A cell-centered scheme is used to store the flow variables. On each cell face the convective and diffusive fluxes are calculated after computing the necessary flow quantities at the face center. Those quantities are obtained by a simple averaging of adjacent cell-center values of the dependent variables.

To maintain stability and to prevent oscillations near shocks or stagnation points, artificial dissipation terms are also included in the viscous calculations. Equation (1) is written in semidiscrete form as

$$\frac{\partial Q}{\partial t} + C(Q) - D(Q) = 0 \tag{2}$$

where the discrete operator C accounts for the physical convective and diffusive terms, whereas D is the operator for the artificial dissipation. The artificial dissipation model used in this paper is basically

the one originally introduced by Jameson et al.[7] To minimize the amount of artificial diffusion inside the shear layer, the eigenvalues scalings of Martinelli and Jameson[8] and Swanson and Turkel[9] have been used to weight these terms. The quantity $D(Q)$ in Eq. (2) is defined as

$$D(Q) = \left(D_\xi^2 - D_\xi^4 + D_\eta^2 - D_\eta^4\right) Q \tag{3}$$

where, for example, in the ξ curvilinear coordinates we have

$$\begin{aligned} D_\xi^2 Q &= \nabla_\xi \left(\Lambda_{i+\frac{1}{2},j} \varepsilon^{(2)}_{i+\frac{1}{2},j}\right) \Delta_\xi Q_{i,j} \\ D_\xi^4 Q &= \nabla_\xi \left(\Lambda_{i+\frac{1}{2},j} \varepsilon^{(4)}_{i+\frac{1}{2},j}\right) \Delta_\xi \nabla_\xi \Delta_\xi Q_{i,j} \end{aligned} \tag{4}$$

where i and j are indices associated with the ξ and η directions, and ∇_ξ and Δ_ξ are forward and backward difference operators in the ξ direction. The variable scaling factor Λ is defined as

$$\Lambda_{i+\frac{1}{2},j} = \tfrac{1}{2}[(\Lambda_\xi)_{i,j} + (\Lambda_\xi)_{i+1,j}] \tag{5}$$

and

$$\Lambda_\xi = \Phi_\xi \lambda_\xi \tag{6}$$

$$\Phi_\xi = 1 + (\lambda_\eta/\lambda_\xi)^\sigma \tag{7}$$

where λ_ξ and λ_η are the scaled spectral radii of the flux Jacobian matrices for the convective terms

$$\lambda_\xi = |U| + a\sqrt{\xi_x^2 + \xi_y^2}, \qquad \lambda_\eta = |V| + a\sqrt{\eta_x^2 + \eta_y^2} \tag{8}$$

and a is the speed of sound. The exponent σ is generally defined by $0 < \sigma \leq 1$, and for two-dimensional applications, a value of 2/3 gives satisfactory results. The coefficients $\varepsilon^{(2)}$ and $\varepsilon^{(4)}$ use the pressure as a sensor for shocks and stagnation points and are defined as follows.

$$\varepsilon^{(2)}_{i+\frac{1}{2},j} = K^{(2)} \max(\nu_{i-1,j}, \nu_{i,j}, \nu_{i+1,j}, \nu_{i+2,j}) \tag{9}$$

$$\nu_{i,j} = \left| \frac{p_{i-1,j} - 2p_{i,j} + p_{i+1,j}}{p_{i-1,j} + 2p_{i,j} + p_{i+1,j}} \right| \tag{10}$$

$$\varepsilon^{(4)}_{i+\frac{1}{2},j} = \max\left[0, \left(K^{(4)} - \varepsilon^{(2)}_{i+\frac{1}{2},j}\right)\right] \tag{11}$$

where typical values for the constants $K^{(2)}$ and $K^{(4)}$ are $\frac{1}{2}$ and $\frac{1}{64}$, respectively. For the other direction, η, the contribution of dissipation is defined in a similar way. The computation of the dissipating terms is carried out in each coordinate direction as the difference between first and third difference operators. Those operators are set to zero on solid walls in order to reduce the global error on the conservation property and to prevent the presence of undamped modes.[9,10]

Boundary Conditions

In cascade-like configurations there are four different types of boundaries: inlet, outlet, solid wall, and periodicity. According to the theory of characteristics, the flow angle, total pressure, total temperature, and isentropic relations are used at the subsonic-axial inlet, whereas the outgoing Riemann invariant is taken from the interior. At the subsonic-axial outlet, the average value of the static pressure is prescribed, and the density and components of velocity are extrapolated.

On the solid walls, the pressure is extrapolated from the interior points, and the no-slip condition and the temperature condition are used to compute density and total energy. For the calculations presented in this paper, all of the walls have been assumed to be at a constant temperature equal to the total inlet one.

Cell-centered schemes are generally implemented using phantom cells to handle the boundaries. Periodicity is, therefore, imposed by setting periodic phantom cell values.

Basic Time-Stepping Scheme and Acceleration Techniques for the Steady Problem

The system of the differential equation (2) is advanced in time using an explicit four-stage Runge–Kutta scheme until the steady-state solution is reached. A hybrid scheme is implemented, where, for economy, the viscous terms are evaluated only at the first stage and then frozen for the remaining stages. If l is the index associated with time, we will write it in the form

$$\begin{aligned} Q^{(0)} &= Q^l \\ Q^{(1)} &= Q^{(0)} + \alpha_1 R(Q^{(0)}) \\ Q^{(2)} &= Q^{(0)} + \alpha_2 R(Q^{(1)}) \\ Q^{(3)} &= Q^{(0)} + \alpha_3 R(Q^{(2)}) \\ Q^{(4)} &= Q^{(0)} + \alpha_4 R(Q^{(3)}) \\ Q^{l+1} &= Q^{(4)} \end{aligned} \tag{12}$$

$$\alpha_1 = \tfrac{1}{4}, \qquad \alpha_2 = \tfrac{1}{3}, \qquad \alpha_3 = \tfrac{1}{2}, \qquad \alpha_4 = 1$$

where the residual $R(Q)$ is defined by

$$R(Q) = \Delta t J[C(Q) - D(Q)] \tag{13}$$

High-frequency damping properties, important for the multigrid process, have been obtained by performing two evaluations of the artificial dissipation terms, at the first and second stages.

To reduce the computational cost, three techniques are employed to speed up convergence to the steady-state solution. These techniques are local time stepping, residual smoothing, and multigrid, they are briefly described in the following subsections.

Local Time Stepping

For steady-state calculations, a faster expulsion of disturbances can be achieved by locally using the maximum allowable time step. In the present work the local time step limit Δt is computed accounting for both the convective (Δt_c) and diffusive (Δt_d) contributions as follows:

$$\Delta t = c_0[\Delta t_c \Delta t_d/(\Delta t_c + \Delta t_d)] \tag{14}$$

where c_0 is a constant usually taken to be the Courant–Friedrichs–Lewy (CFL) number. Specifically, for the inviscid and viscous time step we used

$$\Delta t_c = [1/(\lambda_\xi + \lambda_\eta)] \tag{15}$$

$$\Delta t_d = \frac{1}{K_t(\gamma\mu/\rho Pr) J^2 \left(S_\xi^2 + S_\eta^2\right)} \tag{16}$$

where γ is the specific heat ratio and

$$S_\xi^2 = x_\xi^2 + y_\xi^2, \qquad S_\eta^2 = x_\eta^2 + y_\eta^2 \tag{17}$$

K_t is a constant whose value has been set equal to 2.5 based on numerical experiments.

Residual Smoothing

An implicit smoothing of residuals is used to extend the stability limit and the robustness of the basic scheme. This technique was first introduced by Lerat[11] in 1979 in conjunction with Lax–Wendroff type schemes. Later Jameson[1] implemented this idea on the Runge–Kutta scheme. In two dimensions, the residual smoothing is carried out in the form

$$(1 - \beta_\xi \nabla_\xi \Delta_\xi)(1 - \beta_\eta \nabla_\eta \Delta_\eta)\tilde{R} = R \tag{18}$$

where the residual R includes the contribution of the variable time step and is defined by Eq. (13) and $\tilde{R}$ is the residual after a sequence of smoothing in the ξ and η directions with coefficients β_ξ and β_η. For viscous calculations on highly stretched meshes, the variable

coefficient formulations of Martinelli and Jameson[8] and Swanson and Turkel[9] have been proven to be robust and reliable. In the present paper, the expression for the variable coefficients β of Eq. (18) has been implemented as follows:

$$\beta_\xi = \max\left\{0, \frac{1}{4}\left[\left(\frac{\mathrm{CFL}}{\mathrm{CFL}^*}\frac{\lambda_\xi}{\lambda_\xi+\lambda_\eta}\Phi_\xi\right)^2 - 1\right]\right\}$$
$$\beta_\eta = \max\left\{0, \frac{1}{4}\left[\left(\frac{\mathrm{CFL}}{\mathrm{CFL}^*}\frac{\lambda_\eta}{\lambda_\xi+\lambda_\eta}\Phi_\eta\right)^2 - 1\right]\right\} \tag{19}$$

where the coefficients Φ_ξ and Φ_η are the ones defined in Eqs. (7), and CFL and CFL* are the Courant numbers of the smoothed and unsmoothed scheme, respectively. For the hybrid four-stage scheme we used CFL = 5 and CFL* = 2.5.

Multigrid

This technique was developed for the solution of elliptic problems[12] and later was extended to iperbolic problems.[1,2] The basic idea is to introduce a sequence of coarser grids and use them to speed up the propagation of the fine grid corrections, resulting in a faster expulsion of disturbances. In this work, the full approximation storage schemes of Brandt[12] and Jameson[1] is used.

Coarser auxiliary meshes are obtained by doubling the mesh spacing, and the solution is defined on them using a rule that conserves mass, momentum, and energy:

$$(J^{-1}Q^{(0)})_{2h} = \Sigma(J^{-1}Q)_h \tag{20}$$

where the subscripts refer to the grid spacing, and the sum is over the cells which compose the 2h grid cell. Note that this definition coincides with the one used by Jameson[1] when the reciprocal of the Jacobians are replaced with the cell volumes. To enforce the fine grid approximation, forcing functions P are defined on the coarser grids and added to the governing equations. So, after the initialization of Q_{2h} using Eq. (20), forcing functions P_{2h} are defined as

$$P_{2h} = \Sigma R_h(Q_h) - R_{2h}\left(Q_{2h}^{(0)}\right) \tag{21}$$

and added to the residuals R_{2h} to obtain the value R_{2h}^* that is then used for the stepping scheme:

$$R_{2h}^* = R_{2h}(Q_{2h}) + P_{2h} \tag{22}$$

This procedure is repeated on a succession of coarser grids, and the corrections computed on each coarse grid are transferred back to the finer one by bilinear interpolations.

A V type cycle with subiterations is used as a multigrid strategy. The process is advanced from the fine grid to the coarser one without any intermediate interpolation, and when the coarser grid is reached, corrections are passed back. One Runge–Kutta step is performed on the h grid, two on the 2h grid, and three on all the coarser grids.

For viscous flows with a very low Reynolds number or strong separation, it is important to compute the viscous terms on the coarse grids, too. On coarse grids, the turbulent eddy viscosity is evaluated by averaging the surrounding fine grid values.

On each grid, the boundary conditions are treated in the same way and updated at every Runge–Kutta stage. For economy, the artificial dissipation model is replaced on the coarse grids with constant coefficient second-order differences.

Reformulation of the Governing Equations

Explicit Runge–Kutta schemes in conjunction with residual smoothing and multigrid have been proven very efficient for steady problems. However, those time-dependent methods are no longer time accurate. As shown by Jameson[4] for the Euler equations, the system of Eqs. (1) can be reformulated to be handled by a time-marching steady-state solver. Equations (1) and (2) are rewritten in a compact form as

$$\frac{\partial Q}{\partial t} = -\mathcal{R}(Q) \tag{23}$$

where $\mathcal{R}$ is the residual which includes convective, diffusive, and artificial dissipation fluxes. By the introduction of a fictitious time τ the unsteady governing equations can be reformulated, and a new residual $\mathcal{R}^*$ is defined as

$$\frac{\partial Q}{\partial \tau} = \frac{\partial Q}{\partial t} + \mathcal{R}(Q) = \mathcal{R}^*(Q) \tag{24}$$

Now τ is a fictitious time, and all of the acceleration techniques developed for steady-state computations can be utilized to efficiently reduce the new residual $\mathcal{R}^*$ while marching in τ. Following the approach of Jameson,[4] derivatives with respect to the real time t are discretized using a three-point backward formula that results in an implicit scheme which is second-order accurate in time,

$$\frac{\partial Q}{\partial \tau} = \frac{3Q^{n+1} - 4Q^n + Q^{n-1}}{2\Delta t} + \mathcal{R}(Q^{n+1}) = \mathcal{R}^*(Q^{n+1}) \tag{25}$$

where the superscript n is associated with the real time. Between each time step the solution is advanced in a nonphysical time τ, and acceleration strategies such as local time stepping, implicit residual smoothing, and multigridding are used to speed up the convergence of the residual $\mathcal{R}^*$ to zero to satisfy the time-accurate equations. Boundary conditions are applied explicitly when marching in τ. However, as the system of Eq. (25) is solved for Q^{n+1}, at the end of the iteration in τ the boundary condition will also result, imposed in an implicit manner.

The time discretization of Eq. (25) is fully implicit, however, when solved by marching in τ, stability problems can occur when the stepping in fictitious time τ exceeds the physical one. This generally occurs in viscous calculations where core-flow cells are much bigger then those close to the shear layer. Based on a linear stability analysis of the four-stage scheme of Eq. (12) applied to Eq. (25), the stepping in τ must be less than $\frac{2}{3}\mathrm{CFL}^*\Delta t$. The time step $\Delta\tau$ can then be corrected as follows:

$$\Delta\tau = \min\left(\Delta\tau, \frac{\Delta t}{2^{m-1}(3/2)(\mathrm{CFL}/\mathrm{CFL}^*)}\right) \tag{26}$$

where the contribution of the multigrid speed up is included through 2^{m-1}, m being the total number of grids used in the multigrid process. After limiting the time step $\Delta\tau$ with Eq. (26), the scheme becomes stable, and the physical time step Δt can be chosen safely only on the basis of the accuracy requirement.

At the end of each time step in real time, the time derivative $\partial Q/\partial t$ is updated, and a new sequence in the fictitious time τ is started. Between time steps, multigrid cycles are carried out until the residuals become less then a prescribed value.

To provide a good initialization of the solution at the new time step, a three-point backward formula is used as a predictor:

$$Q^* = Q^n + \frac{3Q^n - 4Q^{n-1} + Q^{n-2}}{2} \tag{27}$$

where Q^* is the predicted value of Q^{n+1}.

It is stressed that using scheme (25) the modifications to turn an existing steady-solution solver to a time-accurate one are quite simple. The time derivative $\partial Q/\partial t$ can be introduced as a source term to be included in the new residual $\mathcal{R}^*$, and the time step is corrected using Eq. (26) to make the scheme stable.

Results and Discussions

The procedure is validated first in two dimensions. Two test cases are presented. First, a vortex shedding over a row of circular cylinders in laminar regime is examined. The interest is mostly in the flow periodicity and in the prediction of the Strouhal number. As a second application of natural unsteadiness, a shock buffeting computation over a bicircular airfoils will be presented. For this case experiments as well as other author's calculations are available for comparison.

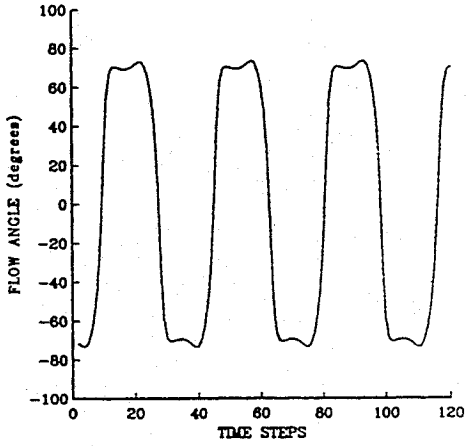

a) Flow angle evolution

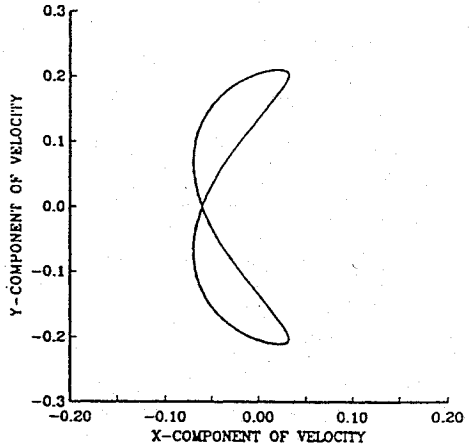

b) Velocity component evolution

Fig. 1 Unsteady flow past a circular cylinder, $M = 0.2$, $Re = 1000$.

Row of Circular Cylinders

This test is intended to predict the natural vortex shedding past a cylinder. A row of circular cylinders in a laminar regime is studied for an inlet flow condition of Mach number 0.2 and Reynolds number of 1000. Calculations were performed on a 257 × 49 elliptic C type grid. The distance between the cylinders is five times the cylinder diameter.

Figures 1a and 1b report the evolution in time of the flow angle and velocity components (phase plot) at a point in the wake close to the cylinder. The time history refers to four cycles of oscillations after a periodic flow condition is reached. The periodic behavior of the flow is evident and proves the robustness and accuracy of the scheme. The time step for those calculations was set to have 40 divisions over a period based on the experimental Strouhal number. This corresponds to a local Courant number between 3 (far field) and 400 (boundary layer). Between time steps, calculations were performed using three grid levels until the root mean square of the norm of residual was less than 10^{-6}. This typically required about 10 multigrid cycles.

The computed Strouhal number based on the inlet velocity is about 0.2 and agrees well with the experimental value of 0.21.

Figure 2 reports the instantaneous streamlines in nine instants over a cycle (the 10th position would be equivalent to the 1st). The shedding of the vortex is very evident as well as the mechanism of their formation with a vortex merging between instants 1 and 2, and 5 and 6.

Shock Buffeting over a Bicircular Airfoil

Starting in 1976 several experiments and calculations were carried out on shock buffeting over a bicircular-arc airfoil. The experiments[13–16] were run at NASA Ames in a wind tunnel specifically designed for this purpose. The facility was aimed to study the

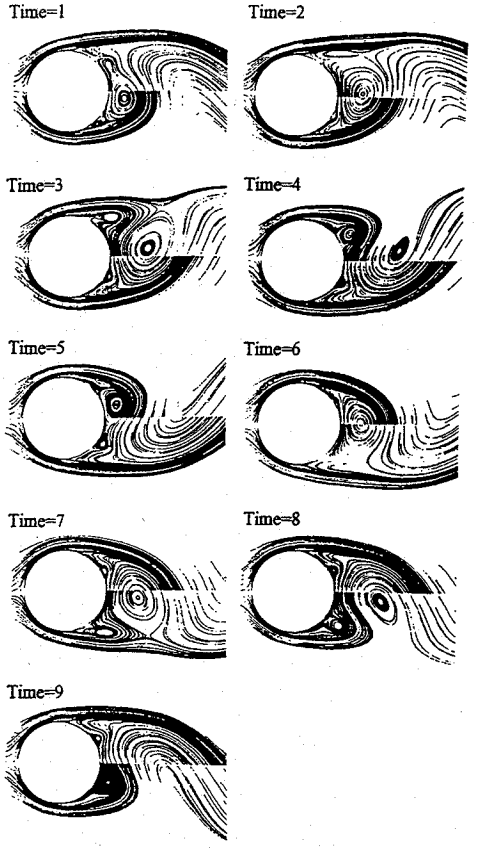

Fig. 2 Instantaneous streamlines for the circular cylinder row test case.

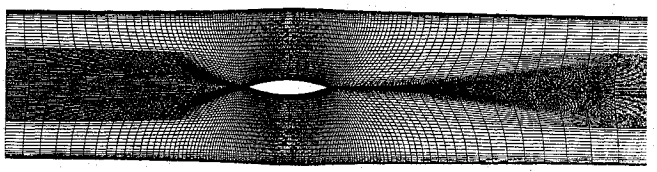

Fig. 3 Computational mesh for the shock buffeting test case, two 161 × 65 H type grid blocks.

flow around a 18% thick airfoil at a nominal test Mach number of 0.775. To reduce upper and lower wall interference effects and to avoid premature choking, the tunnel walls were contoured to follow the airfoil free-air streamlines for the nominal test condition. At a Reynolds number of 7×10^6, experiments suggest buffeting at a freestream Mach number[14] in the range from 0.76 to 0.78 when increasing the Mach number and from 0.78 down to 0.74 when decreasing in speed. Preliminary calculations on a row of bicircular airfoils indicate natural unsteady flow at Mach 0.75. Whereas the flow is produced to be unsteady up to a Mach number of 0.78, the calculation still shows some unsteadiness up to a freestream Mach number of 0.83. The reduced frequency of the experiment is roughly 0.5. Steger,[17] with an isolated airfoil, predicted about 0.41, whereas the TRAF2D code suggested 0.42 for an airfoil distance of 10 times the axial cord. If the airfoils are clustered to a distance of four times the axial cord, the reduced frequency rises to 0.47. Far away from the nominal condition, endwall effects can become important especially at high Mach numbers and so the comparison with a row of airfoils is not too meaningful. It was, therefore, decided to investigate the tunnel configuration by including the contoured tunnel walls in the calculation.

A multiblock version of the TRAF2D code was used for this purpose. Figure 3 shows the computational grid consisting of two blocks of 161 × 65 grid points, where the tunnel walls have been contoured following the data of McDavitt et al.[14] Calculations were performed using three grid levels, and for each time step multigrid cycles were carried out until the root mean square of the norm of residual was less than 10^{-6}. This required from four to eight

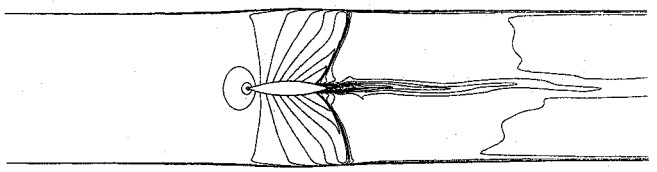

Fig. 4 Instantaneous Mach number contours at choke condition, Mach = 0.785.

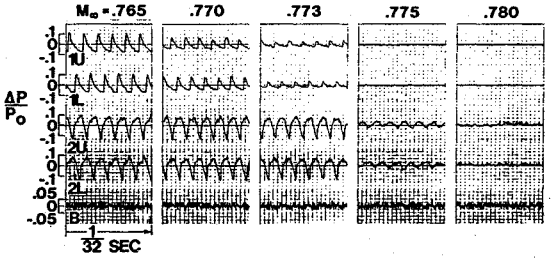

a) Experiment[14] where 1 indicates $x/c = 0.5$, 2 is $x/c = 0.775$, U is upper, and L is lower

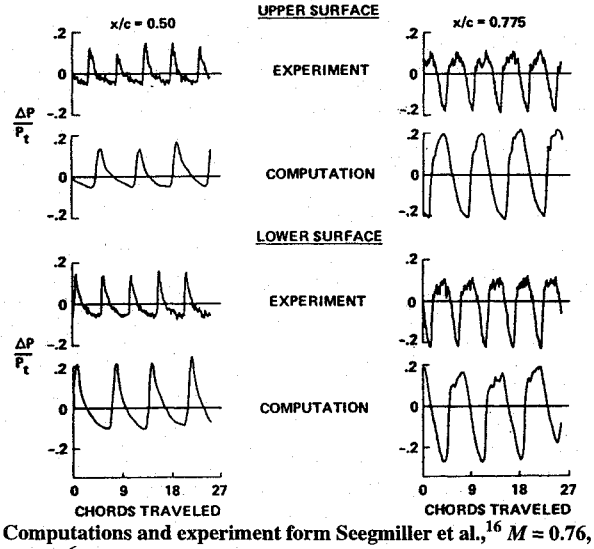

b) Computations and experiment form Seegmiller et al.,[16] $M = 0.76$, $Re = 11 \times 10^6$

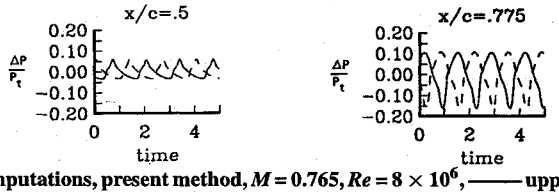

c) Computations, present method, $M = 0.765$, $Re = 8 \times 10^6$, ——— upper, – – – lower

Fig. 5 Unsteady pressure evolution for the shock buffeting test case.

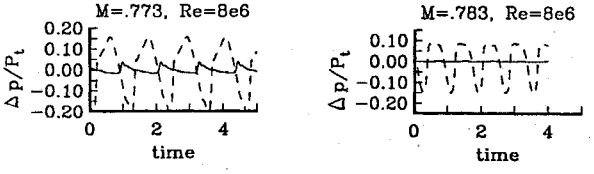

Fig. 6 Unsteady pressure evolution for the shock buffeting test case: ——— $x/c = 0.5$, – – – $x/c = 0.775$.

multigrid cycles between time steps, and 220 s per buffeting cycle on the NASA Lewis CRAY Y-MP. The time step size was chosen to have about 80 divisions within a buffeting period. For that high Reynolds number the Courant number based on 80 divisions within a period was between 1 (far field) and 4000 (boundary layer). The savings in computer time with respect to the purely explicit scheme was 98%.

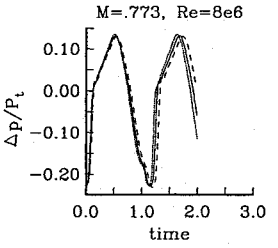

Fig. 7 Unsteady pressure evolution for the shock buffeting test case: – – – 40 divisions, ——— 80 divisions, · · · · · · 160 divisions.

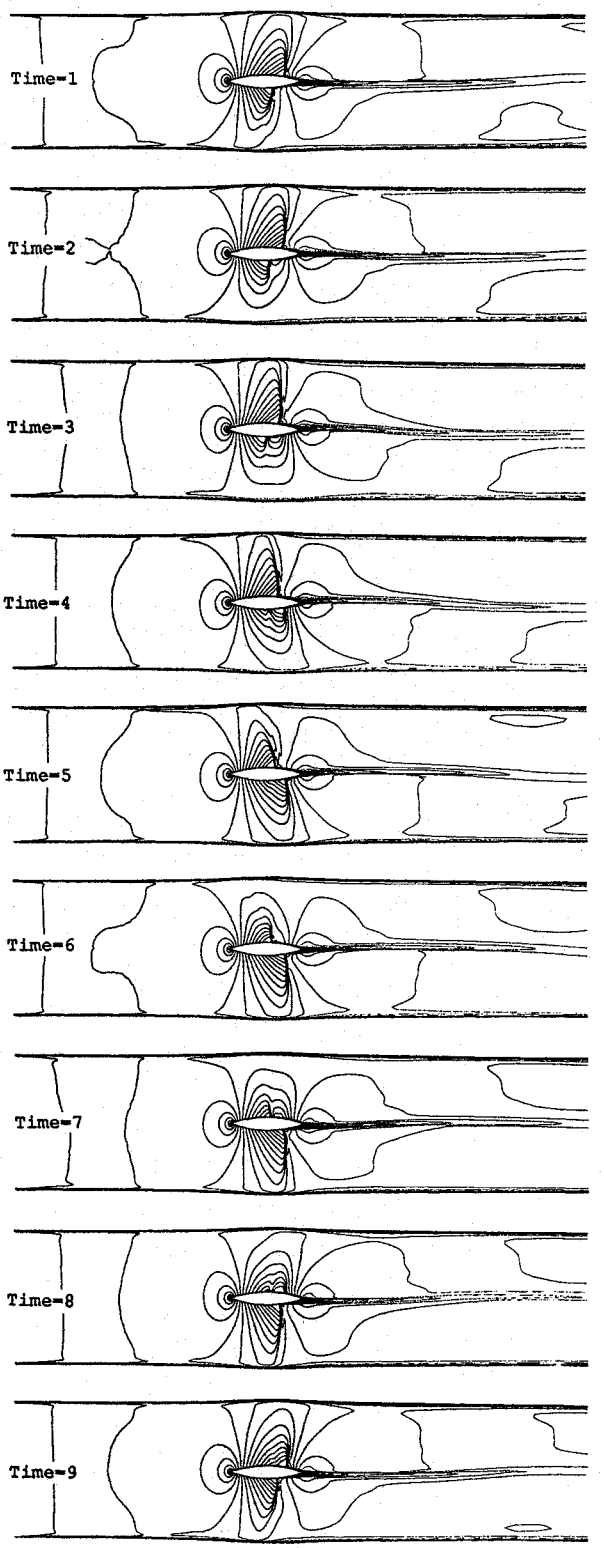

Fig. 8 Instantaneous Mach number contours for the shock buffeting test case; $M = 0.765$, $Re = 8 \times 10^6$.

Shock buffeting was found to occur from a reference Mach number of 0.763 up to 0.783. If the back pressure is decreased, the flow approaches the choke condition (reference Mach number 0.785) and the unsteadiness is confined in the wake, whereas the upper and lower shocks become stable (Fig. 4). The present method indicates a reduced frequency of about 0.41, which is 20% smaller then the experiment but in very good agreement with the calculations of Seegmiller et al.[16]

Figure 5 shows the experimental and computed pressure oscillations at two different locations on the airfoil surface. Calculations from Seegmiller et al.[16] and the present method are included as well. The agreement between the measurement and the calculations is quite good on the whole. The present method underestimates pressure fluctuation about 25% at the first axial position ($x/c = 0.5$) and predicts the right amplitude at $x/c = 0.775$. Seegmiller et al.,[16] with a nonsymmetric code, experienced some overestimation, especially in the second axial position ($x/c = 0.775$). Figure 5c includes pressure fluctuation for both the upper and lower side of the airfoil to show the symmetric behavior of the calculations. In the calculation of the present method, the time has been scaled using the experimental buffeting period.

Figure 6 shows time histories for reference Mach numbers of 0.773 and 0.783, respectively. As the Mach number is increased, fluctuation at the midchord disappear first as the shocks move downstream. Once again, agreement with the experiment (Fig. 5a) is still good, except for the stronger persistency of buffeting, which can be deducted from the plots at $x/c = 0.775$.

The dependency of the pressure evolution on the time step size is investigated in Fig. 7. Calculations were carried out using twice the reference time step and half the reference time step without noting any important impact either on the amplitude or on the frequency of the buffeting. The same analysis was done for the coefficients of the artificial dissipation, and calculations were found again to be substantially independent from those coefficients.

Instantaneous Mach number contours are shown in Fig. 8. The mechanism in the shock buffeting is quite clear. The upper shock moves upstream and increases in intensity (from 1 to 4 times). When the shock reach the position of about 70% of the axial chord, its intensity rapidly decreases (from 5 to 7 times), and a new shock appears before the trailing edge which rapidly moves upstream (from 7 to 9 times). The situation is symmetric on the lower side.

Conclusions

The use of explicit accelerated schemes has been extended to time-accurate Navier–Stokes calculations. In particular, the use of an efficient and highly vectorizable technique such as multigridding is proposed in conjunction with a fully implicit time discretization. A preliminary validation indicates that the approach is robust and efficient. According to the proposed method, the modifications to be made on a time-marching accelerated solver in order to make it time accurate are very simple.

Acknowledgments

The first author would like to express his gratitude to ICOMP and NASA for providing support, facilities, and computer time for this work.

References

[1]Jameson, A., "Transonic Flow Calculations," MAE Report 1651, Mechanical and Aerospace Engineering Dept., Princeton Univ., Princeton, NJ, 1983.

[2]Ni, R.-H., "Multiple-Grid Scheme for Solving the Euler Equations," *AIAA Journal*, Vol. 20, No. 11, 1982, pp. 1565–1571.

[3]Arnone, A., Liou, M.-S., and Povinelli, L. A., "Multigrid Calculation of Three-Dimensional Viscous Cascade Flows," *Journal of Propulsion and Power*, Vol. 9, No. 4, 1993, pp. 605–614.

[4]Jameson, A., "Time Dependent Calculations Using Multigrid, with Applications to Unsteady Flows Past Airfoils and Wings," AIAA Paper 91-1596, June 1991.

[5]Arnone, A., and Swanson, R. C., "A Navier–Stokes Solver for Cascade Flows," NASA CR 181682, July 1988.

[6]Baldwin, B. S., and Lomax, H., "Thin Layer Approximation and Algebraic Model for Separated Turbulent Flows," AIAA Paper 78-257, Jan. 1978.

[7]Jameson, A., Schmidt, W., and Turkel, E., "Numerical Solutions of the Euler Equations by Finite Volume Methods Using Runge–Kutta Time-Stepping Schemes," AIAA Paper 81-1259, June 1981.

[8]Martinelli, L., and Jameson, A., "Validation of a Multigrid Method for the Reynolds Averaged Equations," AIAA Paper 88-0414, Jan. 1988.

[9]Swanson, R. C., and Turkel, E., "Artificial Dissipation and Central Difference Schemes for the Euler and Navier–Stokes Equations," AIAA Paper 87-1107, June 1987.

[10]Pulliam, T. H., "Artificial Dissipation Models for the Euler Equations," *AIAA Journal*, Vol. 24, No. 12, 1986, pp. 1931–1940.

[11]Lerat, A., "Une Classe de Schemas aux Differences Implicites Pour les Systemes Hyperboliques de Lois de Conservation," *Comptes Rendus Hebdomadaires des Seances de l'Academic des Sciences, Series A: Sciences Mathematiques*, Vol. 288A, No. 22, 1979.

[12]Brandt, A., "Multi-Level Adaptive Computations in Fluid Dynamics," AIAA Paper 79-1455, July 1979.

[13]Levy, L. L., "An Experimental and Computational Investigation of the Steady and Unsteady Transonic Flow Field About an Airfoil in a Solid-Wall Test Channel," AIAA Paper 77-678, June 1977.

[14]McDevitt, J. B., Levy, L. L., and Deiwert, G. S., "Transonic Flow About a Thick Circular-Arc Airfoil," *AIAA Journal*, Vol. 14, No. 5, 1976, pp. 606–613.

[15]Levy, L. L., "Experimental and Computational Steady and Unsteady Transonic Flows About a Thick Airfoil," *AIAA Journal*, Vol. 16, No. 6, 1978, pp. 564–572.

[16]Seegmiller, H. L., Marvin, J. G., and Levy, L. L., "Steady and Unsteady Transonic Flow," *AIAA Journal*, Vol. 16, No. 12, 1978, pp. 1262–1270.

[17]Steger, J. L., "Implicit Finite-Difference Simulation of Flow About Arbitrary Two-Dimensional Geometries," *AIAA Journal*, Vol. 16, No. 7, 1978, pp. 679–686.